Development of Advanced Combustion models for Diesel Engines using Large Eddy Simulation

Shrikanth Rao, Eric Pomraning and C. J. Rutland
Engine Research Center, University of Wisconsin – Madison

Presented at the 2nd Joint Meeting of the US Sections of the Combustion Institute, Oakland, CA, March 2001

Abstract

A Probability Density Function (PDF) time-scale combustion model has been developed for simulating diesel combustion and implemented into the KIVA-3V code. Chemical reactions are modeled using a conserved scalar and time-scale approach. A flamelet solution is obtained assuming decoupling of turbulent and chemical time-scales. In order to account for combustion in the distributed reaction regime, we expand the reaction rate about the flamelet solution.

A Dynamic Structure Large Eddy Simulation (LES) turbulence model has been integrated with the PDF time-scale model. The dynamic structure model is a dynamic one-equation non-viscosity model, which captures the flow field more accurately than viscosity-based models and gives better estimates of quantities needed in the combustion model. Model results comparing simulation results against experimental data for a Caterpillar and a Sandia optical access engine are presented. Comparison of the mean stretch rate for a RANS model and the Dynamic Structure LES model are presented for a reacting methane-air jet (Sandia Flame D).

I] Introduction

The goal of combustion modeling is to accurately predict combustion phenomena. In this study, a new PDF time-scale combustion model is presented. The model combines the laminar flamelet combustion model (Peters, 1984) and the characteristic time-scale model (Reitz *et al*., 1983).

Another issue in combustion modeling is accounting for turbulence – scalar interactions. It is believed that Large Eddy Simulation (LES) models are better suited for predicting unsteady turbulent flow than conventional RANS models. Results from a Dynamic Structure LES model (Pomraning, 2000) with the PDF time-scale model are presented.

This paper is organized as follows. First, the PDF timescale model and governing equations are presented. This is followed by the Dynamic Structure LES model and its integration with the PDF time-scale model. Comparisons between a RANS model and the LES model for a reacting gas jet simulation are presented, followed by results from IC engine simulations.

II] PDF Time-scale combustion model

One of the challenges in combustion modeling is evaluating the mean reaction rate term that appears in the species conservation equation. A flamelet approach is used to aid modeling of this term. In diesel engines, the flamelet model must be modified to account for low Damköhler number regions where the assumption of decoupling of turbulent and chemical time-scales is not valid. The PDF time-scale model accounts for these effects using a modified characteristic time-scale approach. Upon combining the flamelet solution with the time-scale approach, the mass fraction of species i at time n+1 is given as:

$$\tilde{Y}^{n+1} = \tilde{Y}_i^* + (\tilde{Y}_i^n - \tilde{Y}_i^*) e^{(-\Delta t/\tau_{chem})}, \tag{2-1}$$

where $\tilde{Y}_i^*$ is the value of the mass fraction obtained from a flamelet solution, and τ_{chem} is a characteristic chemical time-scale obtained by expanding the reaction rate about the flamelet solution. The method for obtaining the flamelet solution and the characteristic time-scale are discussed below.

Under certain assumptions, the species conservation equation can be transformed into mixture fraction space resulting in the flamelet equation, which is given by (Peters, 1984):

$$\rho \frac{\partial Y_i}{\partial t} - \rho \frac{\chi}{2Le_i} \frac{\partial^2 Y_i}{\partial \xi^2} - \dot{\omega}_i = 0. \tag{2-2}$$

Here, ξ is the mixture fraction and χ is a parameter that accounts for both convection and diffusion normal to the surface of stoichiometric mixture fraction, and is defined as:

$$\chi = 2D \frac{\partial \xi}{\partial x_i} \frac{\partial \xi}{\partial x_i}. \tag{2-3}$$

This can be thought of as a reciprocal diffusion time. Since it characterizes the straining/stretching effect on the flame, it is referred to as the stretch rate in this paper.

In this study, the OPPDIF code (Lutz *et al*., 1997) was used to solve the steady flamelet equations governing an opposed jet diffusion flame. A chemical mechanism for octane with 29 species and 48 reactions (Hasse *et al*., 2000) was used. The magnitude of the stretch rate, χ, was varied by varying the fuel and oxidizer velocity boundary conditions. With this information, a library of mean mass fraction of the species as a function of the mean mixture fraction, its variance and the mean stretch rate is computed. The mean mass fractions are determined from the instantaneous OPPDIF solutions by weighting them with a joint PDF for χ and ξ as:

$$\tilde{Y}_i^* = \int_0^\infty \int_0^\infty Y_i(\chi,\xi) P(\chi,\xi)\, d\xi\, d\chi. \tag{2-4}$$

Equation (2-4) is simplified by assuming statistical independence of χ and ξ (Bilger, 1980). This allows the integral in equation (2) to be written as:

$$\tilde{Y}_i^* = \int_0^{\chi_q} \int_0^1 Y_i(\chi,\xi) P_1(\xi) P_2(\chi)\, d\xi\, d\chi, \tag{2-5}$$

where $P_1(\xi)$ is assumed to be a beta distribution and $P_2(\chi)$ is assumed to be a lognormal distribution with a standard deviation of one. Determination of $P_1(\xi)$ requires the mean mixture fraction, $\tilde{\xi}$, and it's variance, $\widetilde{\xi''^2}$. Also, the mean stretch rate, $\overline{\chi}$, is required to determine $P_2(\chi)$. These quantities are determined from LES scalar transport equations discussed in section III.

The mass fractions obtained from equation (2-5) are not valid where the chemical time-scale is equal to or greater than the fluid time-scale. To account for low Damköhler number effects, a modified form of the characteristic time-scale approach of Reitz *et al*. (1983) is used. In this method, the chemical source terms are expanded up to the first order about the flamelet solution using a Taylor series expansion. The time rate of change of species i is then given as:

$$\frac{\partial \tilde{Y}_i}{\partial t} = -\frac{\tilde{Y}_i - \tilde{Y}_i^*}{\tilde{\tau}_{chem}}. \tag{2-6}$$

Upon integrating equation (2-6), we get equation (2-1) for the species mass fraction at time $n+1$.

The characteristic time, τ_{chem}, represents the rate at which each species approaches its flamelet value. This time-scale is currently based on a single step reaction for diesel combustion and is given as:

$$\tau_{chem} = A^{-1} \left(Y_{fuel}\right)^{0.75} \left(Y_{O_2}\right)^{-1.5} \exp\left(\frac{E_A}{RT}\right), \tag{3-1}$$

where $A = 1.54e+10$ and $E_A = 77.3\ kJ/mol$. These values are determined from a one-step reaction-rate expression for tetradecane (Kong et al., 1995). Future work will consider multiple time-scales since each species reacts at a different rate.

In the original formulation of Reitz *et al*. (1983), the reaction rate term is expanded about equilibrium. It should be noted that the current formulation is different from previous time-scale models in that it considers variations about the flamelet solution rather than about equilibrium.

III] Large Eddy Simulation and the Dynamic Structure Model

Large eddy simulation (LES) is based on decomposing a variable into resolved and unresolved components. This is achieved by filtering the governing equations such that the small-scale turbulent motion is excluded from the calculation. This allows large unsteady structures to be resolved and as a result, cycle-to-cycle effects can be captured. The effects of the small-scale motion on the large-scale motion are modeled using sub-grid models.

A Dynamic structure model (Pomraning, 2000) has been implemented into the KIVA-3V code. This LES model is used to evaluate the quantities that are required for the

combustion model. Aspects of this model that are important for the combustion model are presented below.

Sub-Grid Stress Tensor Model

In order to accurately model the combustion process, the effects of turbulent mixing must be modeled correctly. The LES momentum equation for compressible flows is obtained by filtering the Navier-Stokes momentum equation and is given as (Pomraning, 2000):

$$\frac{\partial \overline{\rho}\tilde{u}_i}{\partial t} + \frac{\partial\left(\overline{\rho}\tilde{u}_i\tilde{u}_j\right)}{\partial x_j} = \frac{-\partial \overline{P}}{\partial x_i} + \frac{\partial \overline{\sigma_{ij}}}{\partial x_j} - \frac{\partial \tau_{u_i u_j}}{\partial x_j}, \tag{3-2}$$

where the bar indicates filtering at the grid level and

$$\overline{\sigma_{ij}} = \mu\left(\frac{\partial \widetilde{u_i}}{\partial x_j} + \frac{\partial \widetilde{u_j}}{\partial x_i}\right) - \frac{2}{3}\mu\frac{\partial \widetilde{u_k}}{\partial x_k}\delta_{ij}, \tag{3-3}$$

$$\tau_{u_i u_j} = \overline{\rho}\left(\widetilde{u_i u_j} - \widetilde{u_i}\,\widetilde{u_j}\right), \tag{3-4}$$

and $\tilde{u}_i$ is the LES Favre averaged velocity defined by

$$\tilde{u}_i \equiv \frac{\overline{\rho u_i}}{\overline{\rho}}. \tag{3-5}$$

The sub-grid stress tensor, $\tau_{u_i u_j}$, must be modeled as it cannot be readily determined from the resolved field.

To formulate a dynamic model, a second filtering operation called the 'test' filter is required. The filtering operation at the test level is indicated by the symbol $\widehat{\ }$. The width of the test filter is equal to or greater than the width of the first filter. The second filtering operation results in a stress tensor at the test level, given by

$$T_{ij} = \widehat{\overline{\rho}\widetilde{u_i u_j}} - \widehat{\overline{\rho}}\,\widehat{\widetilde{u}}_i\,\widehat{\widetilde{u}}_j, \tag{3-6}$$

where

$$\widehat{\widetilde{u}}_i = \frac{\widehat{\overline{\rho}\widetilde{u}_i}}{\widehat{\overline{\rho}}}. \tag{3-7}$$

The grid level and test level stress tensors are related by the Germano Identity (Germano, 1991).

$$L_{ij} = T_{ij} - \widehat{\tau_{ij}}, \tag{3-8}$$

where the Leonard stress term, L_{ij}, is given by

$$L_{ij} = \widehat{\overline{\rho}\widetilde{u}_i\widetilde{u}_j} - \widehat{\overline{\rho}}\,\widehat{\widetilde{u}}_i\,\widehat{\widetilde{u}}_j. \tag{3-9}$$

The Leonard stress term can be determined from the resolved field. The Germano identity is useful because it relates the two unknown stress tensors to a known tensor.

In the dynamic structure LES model, the sub-grid stress tensor is modeled directly rather than model it using a viscosity-based approach that is common with other models. Since this model allows for energy flow from the resolved to the sub-grid scales and vice-versa

(i.e. backscatter), an equation for the sub-grid kinetic energy has been added to provide a budget on this energy flow.

In this model, the equation for the sub-grid stress tensor is given by (Pomraning, 2000)

$$\tau_{ij} = c_{ij} k \,, \tag{3-10}$$

and the equation for the test level stress tensor is given by

$$T_{ij} = c_{ij} K \,, \tag{3-11}$$

where the grid level and test level sub-grid kinetic energies are defined by

$$k = \frac{\overline{\rho}}{2}\left(\widetilde{u_i u_i} - \widetilde{u}_i \widetilde{u}_i\right), \tag{3-12}$$

and

$$K = \frac{1}{2}(\widehat{\overline{\rho} u_i u_i} - \widehat{\overline{\rho}} \widetilde{\widehat{u}}_i \widetilde{\widehat{u}}_i) \,. \tag{3-13}$$

The grid level sub-grid kinetic energy is determined from a transport equation, the modeled form of which is given by

$$\frac{\partial k}{\partial t} + \frac{\partial \widetilde{u}_j k}{\partial x_j} = \frac{\partial}{\partial x_j}\left(\nu \frac{\partial k}{\partial x_j}\right) - \tau_{ij} \widetilde{S}_{ij} - \varepsilon \tag{3-14}$$

The grid and test level sub-grid kinetic energies are related by the trace of the Leonard term in equation (3-9) as

$$K = \widehat{k} + \frac{1}{2} L_{ii} \,. \tag{3-15}$$

The tensor structure of the sub-grid stresses is obtained from the tensor coefficient c_{ij}, which is found using the Germano identity. It is assumed that the tensor coefficient is the same at both filter levels. Substituting the models for the stress tensors into the Germano identity gives

$$L_{ij} = K c_{ij} - \widehat{k c_{ij}} \,. \tag{3-16}$$

An algebraic form of the model is obtained by assuming that the tensor coefficient can be removed from the integral in equation (3-16) and solving for τ_{ij} which gives

$$\tau_{ij} = L_{ij}\left(\frac{2k}{L_{kk}}\right). \tag{3-17}$$

Models for the unclosed terms in equation (3-14) are discussed by Pomraning (2000). These models were validated using DNS data.

LES Scalar Transport

As discussed in section II, determination of the mean species fractions requires the mean mixture fraction, its variance, and the mean stretch rate. In order to obtain these quantities, transport equations are solved for the mean mixture fraction and sub-grid mixture fraction fluctuations. The filtered LES equation for the Favre-averaged mixture fraction, $\widetilde{\xi}$, is given as:

$$\frac{\partial \overline{\rho}\tilde{\xi}}{\partial t}+\frac{\partial \overline{\rho}\widetilde{u_i}\tilde{\xi}}{\partial x_i}=-\frac{\partial \tau_{u_i\xi}}{\partial x_i}+\overline{\frac{\partial}{\partial x_i}D\rho\frac{\partial \xi}{\partial x_i}}, \tag{3-18}$$

where the sub-grid scalar-flux is given by

$$\tau_{u_i\xi}=\overline{\rho}\left(\widetilde{u_i\xi}-\widetilde{u_i}\,\tilde{\xi}\right), \tag{3-19}$$

which needs to be modeled. This term is modeled using a gradient approximation as:

$$\tau_{u_i\xi}=-\mu_s\frac{\partial \tilde{\xi}}{\partial x_i}, \tag{3-20}$$

where μ_s is a scalar transport coefficient determined as:

$$\mu_s=c_k\Delta k^{1/2}. \tag{3-21}$$

Here c_k is set to the value of 0.05 (Menon *et al.,* 1996*)* and Δ is the filter width of the grid-level filter.

The combustion model also requires the mean stretch rate and the variance of the mixture fraction. In order to evaluate these quantities, a transport equation for the sub-grid mixture fraction fluctuations is solved. The modeled form of this equation is given by

$$\frac{\partial \Phi}{\partial t}+\frac{\partial \widetilde{u_i}\,\Phi}{\partial x_i}=-\frac{\partial \tau_{u_i\Phi}}{\partial x_i}+2\tilde{\xi}\frac{\partial \tau_{u_i\phi}}{\partial x_i}+\frac{\partial}{\partial x_i}\left(D\frac{\partial \Phi}{\partial x_i}\right)-\overline{\rho}\chi \tag{3-22}$$

where

$$\Phi=\overline{\rho}\left(\widetilde{\xi\xi}-\tilde{\xi}\tilde{\xi}\right), \tag{3-23}$$

$$\tau_{u_i\Phi}=\overline{\rho}\left(\widetilde{u_i\xi\xi}-\widetilde{u_i}\,\widetilde{\xi\xi}\right), \tag{3-24}$$

and

$$\chi=2D\left(\widetilde{\frac{\partial \xi}{\partial x_i}\frac{\partial \xi}{\partial x_i}}-\frac{\partial \tilde{\xi}}{\partial x_i}\frac{\partial \tilde{\xi}}{\partial x_i}\right). \tag{3-25}$$

The dissipation term for sub-grid mixture fraction fluctuations, χ, is modeled as:

$$\chi=\frac{\Phi}{L_\Phi}L_\chi, \tag{3-26}$$

where

$$L_\chi=2D\left(\widetilde{\overline{\rho}\frac{\partial \tilde{\xi}}{\partial x_j}\frac{\partial \tilde{\xi}}{\partial x_j}}-\hat{\overline{\rho}}\,\widehat{\frac{\partial \tilde{\xi}}{\partial x_j}\frac{\partial \tilde{\xi}}{\partial x_j}}\right), \tag{3-27}$$

$$L_\Phi=\widetilde{\overline{\rho}\tilde{\xi}\tilde{\xi}}-\hat{\overline{\rho}}\,\hat{\tilde{\xi}}\hat{\tilde{\xi}}, \tag{3-28}$$

and

$$\hat{\tilde{\xi}}=\frac{\widehat{\overline{\rho}\tilde{\xi}}}{\hat{\overline{\rho}}} \tag{3-29}$$

Methods for modeling the other unclosed terms in equation (3-22) are discussed by Pomraning (2000).

The mean stretch rate $\overline{\chi}$, given by averaging equation (2-3), is:

$$\overline{\chi} = 2D\overline{\frac{\partial \xi}{\partial x_i}\frac{\partial \xi}{\partial x_i}}. \tag{3-30}$$

This is determined from equation (3-25) as:

$$\overline{\chi} = \chi + 2D\frac{\partial \tilde{\xi}}{\partial x_i}\frac{\partial \tilde{\xi}}{\partial x_i}, \tag{3-31}$$

It can be seen that as grid resolution increases, this term approaches the instantaneous stretch rate defined in equation (2-3). This offers an improvement over RANS models, which are known to do a poor job of predicting $\overline{\chi}$ (Peters *et al.,* 1988).

Equation (3-22) is also used to determine the variance of the mixture fraction. The relation, $\widetilde{\xi'\xi'} = \widetilde{\xi\xi} - \tilde{\xi}\tilde{\xi}$, which is true in a RANS model is not valid for LES averaging since, in general, for LES, $\widetilde{\xi'} \neq 0$. However, the two quantities, $\widetilde{\xi'\xi'}$ and $\widetilde{\xi\xi} - \tilde{\xi}\tilde{\xi}$ have the same qualitative trend as they tend to be large in regions of large gradients. Therefore, it is assumed that the quantity $\widetilde{\xi\xi} - \tilde{\xi}\tilde{\xi}$ can be used in place of $\widetilde{\xi'\xi'}$ to determine the PDF of ξ. Knowing $\tilde{\xi}$ from equation (3-18), $\widetilde{\xi\xi} - \tilde{\xi}\tilde{\xi}$ from equation (3-22), and $\overline{\chi}$ from equation (3-31) allows us to determine mean species mass fractions using equation (2-4).

IV] Results and Discussion

Reacting Jet Simulation

RANS and LES simulations of a turbulent reacting methane – air jet (TNF Website and Barlow *et al*., 1998), known as the Sandia D flame, have been performed. The experimental setup consists of a main fuel jet of diameter 7.2 mm. The main jet composition is 25% methane and 75% air. The main jet is surrounded by a burnt-gas pilot of diameter 18 mm. The temperature of the burnt gases is approximately 1880 K and their composition is known. The pilot stream is surrounded by an air co-flow. The Reynolds number based on the fuel stream is 22400.

These simulations need to be run longer before comparisons of mean scalar quantities can be made against experimental values; however, some conclusions can be drawn from the results obtained so far. Images of the mean stretch rate and mean temperature up to 35 main jet diameters downstream of the jet inlet and 20 main jet diameters in the radial direction are shown in figure 1.

It is seen that the stretch rate predicted by the RANS simulation is high in regions of high shear. However, studies on opposed flow diffusion flames show that the stretch rate is highest in the reaction zone as gradients of mixture fraction are large in this region. The LES simulation picks up large stretch rates in the reaction zone (regions of high temperatures), which agrees with simulations of opposed flow diffusion flames. It is

important to predict the stretch rate correctly in order to correctly predict phenomena such as local extinction.

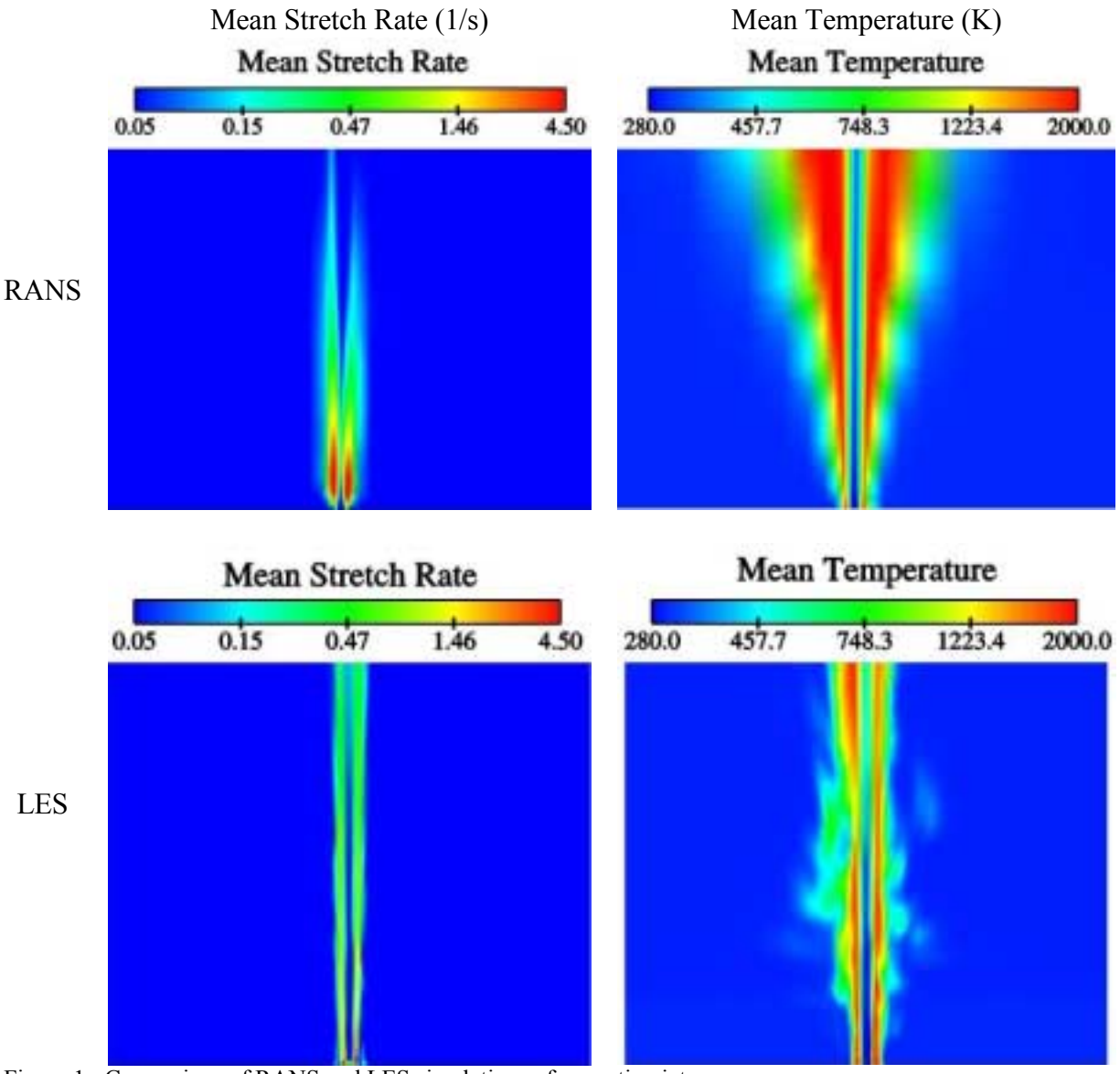

Figure 1: Comparison of RANS and LES simulations of a reacting jet

Engine Simulations

Engine simulations for a Caterpillar 3400 Series Engine and a Sandia Optical access engine (Dec, 1997) using 60º-sector meshes were performed. An engine simulation for a Caterpillar series engine using a 360º-cartesian mesh was also performed.

Pressure traces from engine simulations using the sector mesh are presented in figure 2. The operating conditions for the engines are shown in table 1.

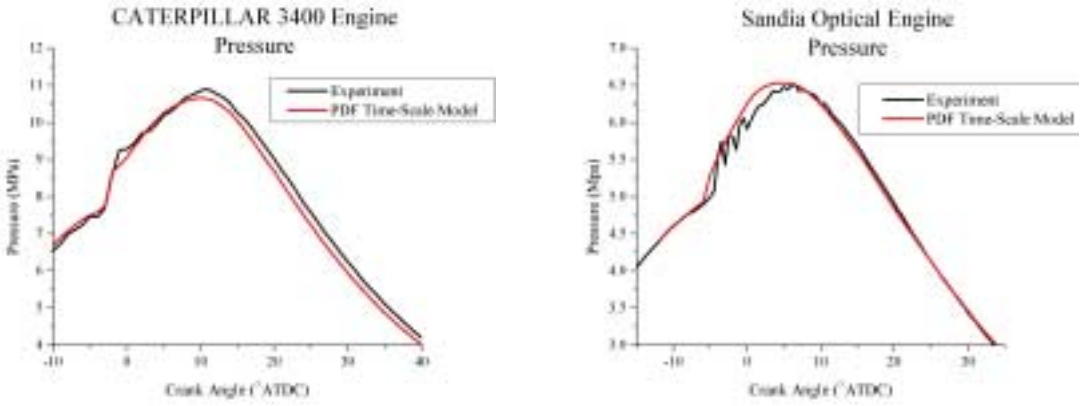

Figure 2: Pressure Traces for Caterpillar and Sandia Engine

Engine	Speed (rpm)	θ_{INJ} (CA° ATDC)	$\dot{m}_{fuel}$	P_{in} (kPa)
Caterpillar	1600	-9.0	129 g/min	183
Sandia	1200	-11.5	0.0535 g/cycle	206

Table 1: Engine Operating Conditions

It is seen that good agreement is obtained for both these engines. The model is able to correctly predict the phasing of the pressure rise and fall and the sharp rise in pressure due to the premixed burn. The constant C_k in equation (3-21) had to be changed to 0.3 for these cases. These had to be changed because a 60º-sector mesh was used. Since the periodic boundaries are close to each other near the nozzle tip in the sector mesh, large eddies cannot be formed in this region and enough turbulent mixing is not generated. In order to generate the turbulent mixing, additional viscosity is added by increasing the scalar transport coefficient.

Figure 3 show simulations performed using a 360° Cartesian mesh as compared to simulations using a 60° sector mesh. The figure shows the spray droplets and the temperature distribution in the engine cylinder.

360º Cartesian Mesh

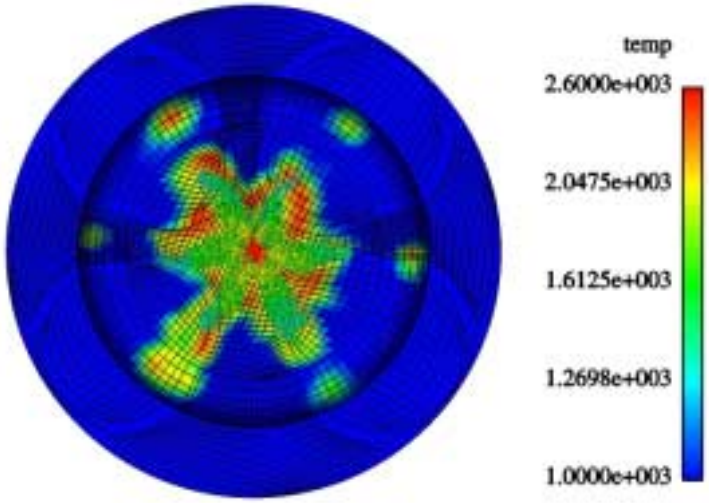

60º Sector Mesh

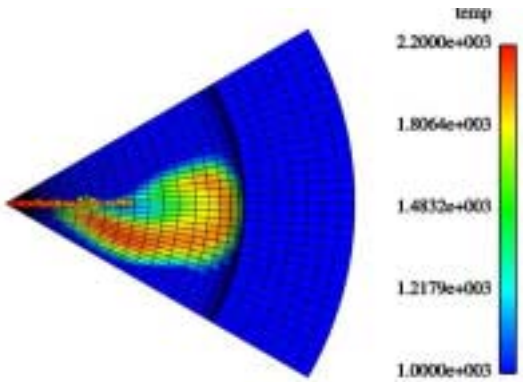

Figure 3: Comparison of sector mesh and cartesian mesh

More evidence of large-scale structure is seen in results from the 360º Cartesian Mesh than in results from the 60º Sector Mesh. The lack of symmetry in droplet distribution for the six spray plumes and in the temperature distribution around these spray plumes is evident when using the cartesian mesh. This indicates that the fuel vapor spreads in a non-symmetric manner in the combustion chamber.

A pressure trace for the case using the cartesian mesh is shown in figure 4 and in this case, good agreement was obtained without changing the constant. As with the sector meshes, in this case, the combustion model predicts the intial sharp rise in pressure and also correctly predicts the crank angle at which the peak pressure occurs.

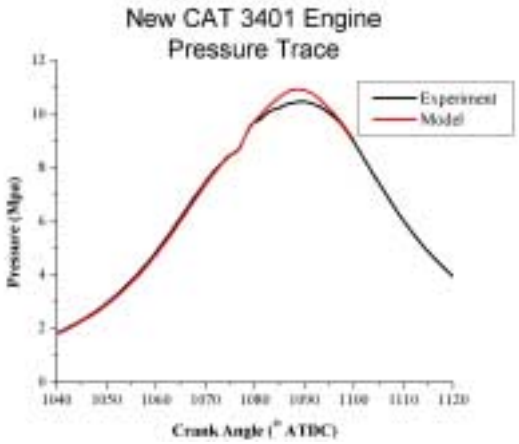

Figure 4: Pressure trace for simulation with cartesian mesh

V] Conclusions

A PDF time-scale combustion model has been developed for diesel combustion. This model can be used in all regimes of combustion without the need for a separate premixed combustion model. The combustion model has been integrated with a dynamic structure LES turbulence model. Results from engine simulations show that the PDF time-scale model with the LES model can predict combustion in diesel engines with a fair degree of accuracy. Preliminary results also show that this model could be used for simulating jet flames and progress in this direction is currently underway.

References

Amsden A.A., (1997), "KIVA-3V: A Block-structured KIVA program for Engines with Vertical or Canted Valves", LA-13313-MS, July

Barlow, R.S. and Frank, J.H., (1998), "Effect of turbulence on species mass fractions in methane/air jet flames", Proc. Combust. Inst., 27:1087-1095

Bilger, R.W., (1980), Turbulent Reacting Flows (Libby, P.A., and Williams, F.A., Editors) Spring-Verlag

Dec, J., (1997), "A Conceptual Model of DI Diesel Combustion Based on Laser-Sheet Imaging", SAE Technical Paper No. 970873

Germano M., Piomelli U., Moin P., and Cabot W. H. (1991), "A Dynamic Subgrid-Scale Eddy Viscosity Model," Physics of Fluids A, Vol. 3, No. 7, pp. 1760-1765

Hasse, C., Bollig, M., and Peters, N., (2000), "Quenching of Laminar Iso-Octane Flames at Cold Walls", Combustion and Flame, 122:117-129

Kong S.C., Zhiyu Han, and Reitz R.D. (1995), "The Development and Application of a Diesel Ignition and Combustion Model for Multidimensional Engine Simulation", SAE Technical Paper No. 950278

Lutz, A., Kee, R., Grcar, J., and Rupley, F., (1997), "OPPDIF: A Fortran Program for Computing Opposed-flow Diffusion Flames", SANDIA National Laboratory Report #SAND96-8243 UC-1409, May

Menon S., Yeung P. K., and Kim W. W., (1996), "Effect of Subgrid Models on the Computed Interscale Energy Transfer in Isotropic Turbulence," Computer and Fluids, Vol. 25, No. 2, pp. 165-180

Peters N. (1984), "Laminar Diffusion Flamelet Models in Non-Premixed Turbulent Combustion", Progress in Energy and Combustion Science, Vol. 10, pp 319-339

Peters N., and Effelsberg E., (1988), "Scalar Dissipation Rates in Turbulent Jets and Jet Diffusion Flames", 22nd Symposium (International) on Combustion, The Combustion Institute, pp. 693-700

Pomraning Eric (2000), Ph.D. Thesis, Engine Research Center, University of Wisconsin-Madison

Reitz R.D., and Bracco F.V. (1983), "Global Kinetics Models and Lack of Thermodynamic Equilibrium", Combustion and Flame 53:141-143

TNF Website, International Workshop on Measurement and Computation of Turbulent Non-premixed Flames, http://www.ca.sandia.gov/tdf/3rdWorkshop/M3APilot97/FlameD.html